

Article

Lipopolysaccharide induces placental mitochondrial dysfunction in murine and human systems by reducing MNRR1 levels via a TLR4-independent pathway

Neeraja Purandare,^{1,5} Yusef Kunji,⁵ Yue Xi,⁸ Roberto Romero,^{1,3,4,5,6} Nardhy Gomez-Lopez,^{1,2,7} Andrew Fribley,⁸ Lawrence I. Grossman,^{1,5,9,*} and Siddhesh Aras^{1,5,*}

SUMMARY

Mitochondria play a key role in placental growth and development, and mitochondrial dysfunction is associated with inflammation in pregnancy pathologies. However, the mechanisms whereby placental mitochondria sense inflammatory signals are unknown. Mitochondrial nuclear retrograde regulator 1 (MNRR1) is a bi-organellar protein responsible for mitochondrial function, including optimal induction of cellular stress-responsive signaling pathways. Here, in a lipopolysaccharide-induced model of systemic placental inflammation, we show that MNRR1 levels are reduced both in mouse placental tissues *in vivo* and in human trophoblastic cell lines *in vitro*. MNRR1 reduction is associated with mitochondrial dysfunction, enhanced oxidative stress, and activation of pro-inflammatory signaling. Mechanistically, we uncover a non-conventional pathway independent of Toll-like receptor 4 (TLR4) that results in ATM kinase-dependent threonine phosphorylation that stabilizes mitochondrial protease YME1L1, which targets MNRR1. Enhancing MNRR1 levels abrogates the bioenergetic defect and induces an anti-inflammatory phenotype. We therefore propose MNRR1 as an anti-inflammatory therapeutic in placental inflammation.

INTRODUCTION

Under healthy conditions, mitochondria are required to generate energy for cellular functioning in the form of ATP. This process is fine-tuned to respond to stress signals by slowing ATP production and activating immune response pathways such as by generating reactive oxygen species (ROS) (West et al., 2011) and other biological processes (Tiku et al., 2020). The role of placental mitochondria has only recently been reported in normal gestation (Holland et al., 2017; Sferruzzi-Perri et al., 2019). Yet, mitochondrial dysfunction has been associated with pregnancy complications including intrauterine growth restriction (Mando et al., 2012), maternal adiposity (Mele et al., 2014; Roberts et al., 2009), gestational diabetes (Wang et al., 2019), preeclampsia (Muralimanoharan et al., 2012; Yung et al., 2019), and spontaneous preterm birth (Panfoli et al., 2016), of which the latter two conditions are associated with inflammatory responses in the placental tissues (Gomez-Lopez et al., 2019). However, the mechanisms whereby placental mitochondria sense inflammatory signals at a cellular and mechanistic level are not clearly known.

We previously showed that mitochondrial nuclear retrograde regulator 1 (MNRR1) (also CHCHD2; AAG10, PARK22) regulates mitochondrial function by acting in two compartments—the mitochondria and the nucleus (Aras et al., 2013, 2015, 2017; Purandare et al., 2018). MNRR1 interacts with complex IV (cytochrome c oxidase; COX) of the electron transport chain (ETC) to regulate oxygen consumption and can alter apoptosis by interacting with Bcl-xL (Liu et al., 2015). In the nucleus, MNRR1 regulates the transcription of numerous genes including subunits of ETC complexes, ROS scavenger genes, and proteins that regulate mitochondrial proliferation (Aras et al., 2015, 2020; Madrid et al., 2020). Here, we have characterized the role of MNRR1 *in vivo* using placental tissues from a murine model of lipopolysaccharide (LPS)-induced preterm birth and *in vitro* using cultured trophoblast (i.e., placental) cell lines. We found that LPS reduces MNRR1 levels in placental tissue as well as in trophoblast cell lines. We then went on to identify a novel pathway that results in MNRR1-dependent mitochondrial dysfunction, thereby uncovering potential new therapeutic targets. Taken together, our work shows that MNRR1 plays a protective role not only by

¹Perinatology Research Branch, Division of Obstetrics and Maternal-Fetal Medicine, Division of Intramural Research, Eunice Kennedy Shriver National Institute of Child Health and Human Development, National Institutes of Health, U.S. Department of Health and Human Services (NICHD/NIH/DHHS), Bethesda, MD 20892, Detroit, MI 48201, USA

²Department of Obstetrics and Gynecology, Wayne State University School of Medicine, Detroit, MI 48201, USA

³Department of Obstetrics and Gynecology, University of Michigan, Ann Arbor, MI 48104, USA

⁴Department of Epidemiology and Biostatistics, Michigan State University, East Lansing, MI 48824, USA

⁵Center for Molecular Medicine and Genetics, Wayne State University; Detroit, MI 48201, USA

⁶Detroit Medical Center, Detroit, MI 48201, USA

⁷Department of Biochemistry, Microbiology, and Immunology, Wayne State University School of Medicine, Detroit, MI 48201, USA

⁸Department of Pediatrics, Wayne State University School of Medicine, Detroit, MI 48201, USA

⁹Lead contact

*Correspondence: lgrossman@wayne.edu (L.I.G.), saras@wayne.edu (S.A.)

<https://doi.org/10.1016/j.isci.2022.105342>



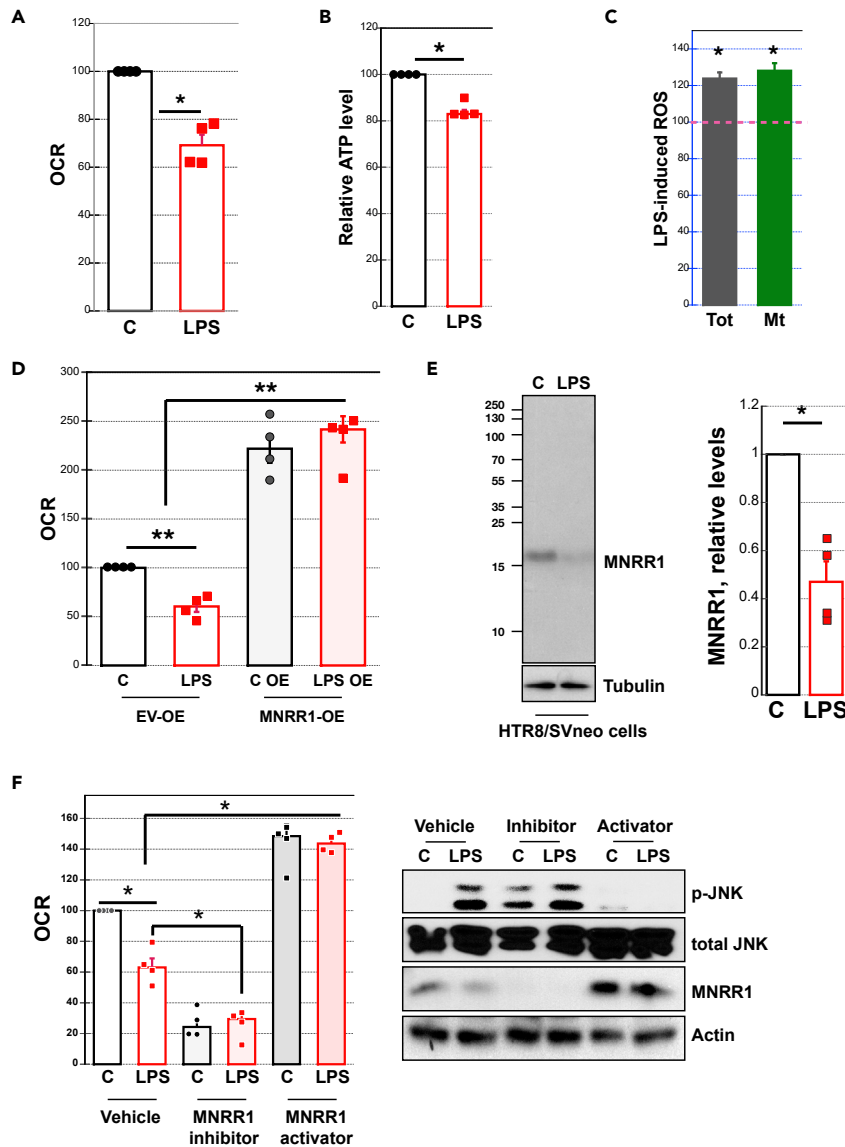


Figure 1. LPS decreases MNRR1 levels and impairs mitochondrial function in human placental cells, defects that can be rescued by increasing MNRR1 expression

All LPS treatments in cultured cells are at 500 ng/mL for 24 h unless indicated otherwise. In all figures: *, $p < 0.05$; **, $p < 0.005$.

(A) Intact cellular oxygen consumption rate (OCR) in the HTR cells treated with control (water) or LPS. Data are represented as oxygen consumption relative to control set to 100% ($n = 4$ biological replicates).

(B) Equal numbers of HTR cells were plated in a 96-well plate and ATP levels were measured ($n = 4$ biological replicates).

(C) HTR cells were treated with control (water; set to 100) or LPS and ROS levels were measured using CM-H₂DCFDA (total amount (Tot), Ex: 485 nm/Em: 527 nm) or MitoSOX Red (mitochondrial amount (Mt), Ex: 510 nm/Em: 580 nm) ($n = 4$ biological replicates).

(D) Intact cellular oxygen consumption in HTR cells overexpressing (OE) EV (empty vector) or MNRR1 and treated with control (water) or LPS. Data are represented as oxygen consumption relative to EV (empty vector) control set to 100 ($n = 4$ biological replicates).

(E) *Left*, Equal amounts of HTR cells treated with control (water) or LPS were separated on an SDS-PAGE gel and probed for MNRR1 levels. Tubulin was probed as a loading control. *Right*, the graph represents MNRR1 levels relative to tubulin ($n = 4$ biological replicates).

Figure 1. Continued

(F) *Left*, Intact cellular oxygen consumption in HTR cells treated with Vehicle (DMSO), MNRR1 inhibitor (Clotrimazole, 10 μ M), or MNRR1 activator (Nitazoxanide, 10 μ M) with control (water) or LPS (500 ng/mL) for 24 h. Data are expressed relative to EV control set to 100 ($n = 4$ biological replicates). *Right*, Pooled lysates from OCR measurement were separated on an SDS-PAGE gel and probed for MNRR1, phospho-JNK, and total JNK levels. Actin was probed as a loading control.

activating mitochondrial function but also by inducing an anti-inflammatory response to ameliorate the deleterious effects of placental inflammation.

RESULTS**LPS-induced reduction in MNRR1 levels impairs mitochondrial function in HTR8/SVneo human placental cells *in vitro***

MNRR1 modulates several mitochondrial functions including oxygen consumption, ATP production, and generation of ROS (Aras et al., 2015). To analyze these effects in a human system *in vitro*, we generated a placental cell culture model of LPS-induced inflammation using the trophoblast cell line HTR8/SVneo (HTR). Because inflammation suppresses mitochondrial function (Stavru et al., 2011), we first determined the effect of inflammation on MNRR1 in these placental cells. When we measured the basal oxygen consumption rate (OCR) in intact trophoblast cells treated with LPS, we found a \sim 30% decrease along with an \sim 18% reduction in cellular ATP levels (Figures 1A and 1B). Furthermore, both total intracellular ROS and mitochondrial ROS were increased (Figure 1C). The decrease in OCR can be completely rescued (and enhanced) by overexpressing WT-MNRR1 (Figure 1D). The decrease in OCR due to LPS is consistent with the observation that MNRR1 levels are reduced in LPS-treated placental cells (Figure 1E). This reduced OCR has also been shown in MNRR1-depleted cells (Aras et al., 2015). A similar reduction in protein levels of MNRR1 was observed in other human placental cells (Figure S1A) as well as non-placental cell lines (data not shown). The reduction in MNRR1 is a post-translational effect as no changes in transcript or promoter reporter levels were observed (Figure S1B). To further link MNRR1 levels with mitochondrial function, we inhibited MNRR1 expression pharmacologically (clotrimazole), which sensitized cells to the effect of LPS on OCR (Figure 1F (left), bars 3 and 4) and an activator (nitazoxanide), which prevented these effects (Figure 1F (left), bars 5 and 6). These compounds were identified using a high-throughput screen for compounds modulating MNRR1 transcription (data not shown). We also examined the effects of MNRR1 inhibition and activation on cellular inflammation by assessing JNK phosphorylation (Figure 1F (right)). Chemical inhibition of MNRR1 acts similarly to LPS-mediated inflammation in increasing JNK phosphorylation (Figure 1F (right)). Importantly, chemical activation of MNRR1 by nitazoxanide prevents this increase even after LPS treatment (Figure 1F, right; Figure S1C), suggesting that such activators could be repurposed therapeutically to treat placental inflammation.

MNRR1 levels are also reduced in a murine bacterial endotoxin model of placental inflammation *in vivo*

To assess the *in vivo* relevance of our observations in cultured placental cells, we utilized a mouse model of LPS-induced systemic inflammation. LPS treatment is known to induce a high rate of preterm labor and birth (Gomez-Lopez et al., 2018). Our examination of MNRR1 protein levels in placental lysates from LPS-treated mice showed them to be significantly decreased (Figure 2A). Reduced MNRR1 levels were also observed by immunohistochemistry of mouse placental tissue injected with LPS (Figure 2B). No change in the transcript levels of MNRR1 was observed in mouse placental tissues (Figure S1D), suggesting a post-translational effect.

We also tested a human placental tissue sample from a patient with clinical chorioamnionitis (Oh et al., 2017) who delivered preterm. In this sample, we found MNRR1 levels considerably reduced in the villous layer of the placenta and moderately so in the base plate (Figure 2C). Our data with both mouse and human placental samples thus suggest that MNRR1 reduction occurs in response to maternal systemic inflammation.

Increased YME1L1 protease reduces mitochondrial MNRR1 levels in human placental cells *in vitro*

Because MNRR1 is a bi-organellar protein that is localized both to the mitochondria and the nucleus (Aras et al., 2015, 2017; Purandare et al., 2018), we determined the effect of LPS on MNRR1 levels in each of the compartments. We found that most of the decrease at the protein level was accounted for by mitochondrial MNRR1 (Figure 3A), strikingly so when visualized by confocal microscopy (Figure 3B). To investigate how

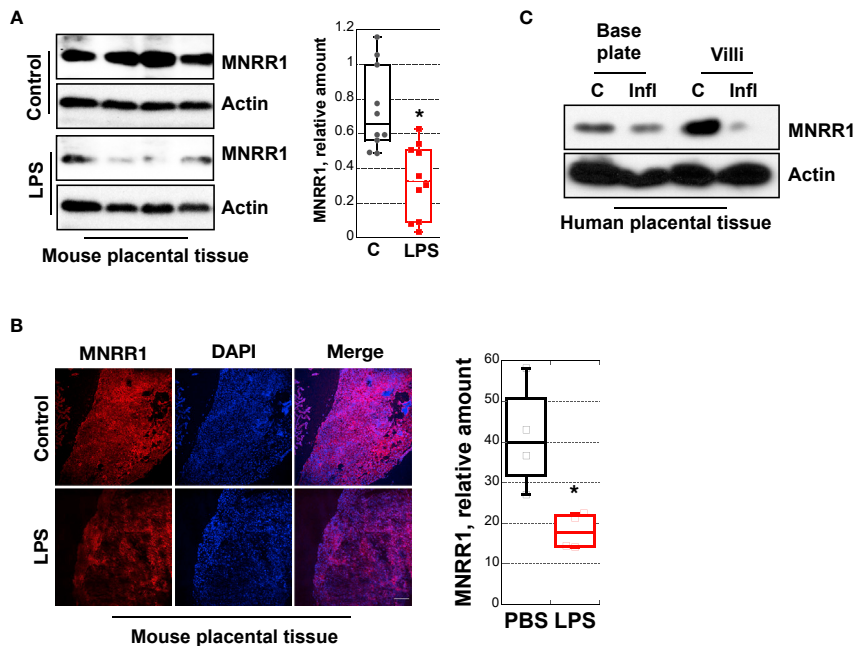


Figure 2. MNRR1 protein levels are reduced in vivo in placental inflammation

(A) *Left*, Placental lysates from control (PBS) versus LPS (intraperitoneally) injected mice were separated on an SDS-PAGE gel and probed for MNRR1 levels. Actin was used as a loading control. *Right*, MNRR1 levels relative to Actin (n = 10 animals per group).

(B) *Left*, Placental tissue sections from control (PBS) versus LPS-injected mice analyzed using immunofluorescence staining. Scale bar represents a distance of 100 μ m. *Right*, Relative MNRR1 fluorescence is shown (n = 4 animals per group).

(C) Equal amounts of human placental lysates from an individual without inflammation (C) and one with systemic inflammation (Infl) were separated on SDS-PAGE gel and probed for MNRR1. Actin was probed as a loading control.

the mitochondrial reduction in MNRR1 takes place, we assessed the protein levels of YME1L1, a mitochondrial intermembrane space (IMS) protease we previously showed to be responsible for the turnover of mitochondrial MNRR1 (Aras et al., 2020). We found that levels of YME1L1 are significantly increased by LPS treatment (Figure 3C) without any change in the transcript levels (Figure S2A). To evaluate whether YME1L1 is required for the LPS-induced effect on MNRR1, we used a HEK293 cell model (which responds to LPS, resulting in a reduction of MNRR1) containing a knockout of YME1L1 (YME1L1-KO). LPS treatment reduced the levels of MNRR1 in the wild type but not the YME1L1-KO cells (data not shown). The levels of OMA1, another protease that has been identified to turn over MNRR1 under cellular stress (Liu et al., 2020), are not increased with LPS treatment in HTR8/SVneo (Figure S2B), thereby suggesting that the upstream inflammatory signaling pathway involves only YME1L1. To further define the role of YME1L1 in regulating MNRR1 levels in mitochondria, we utilized a version of YME1L1 mutated to eliminate protease activity (protease-dead; PD) (MacVicar et al., 2019). In HTR8/SVneo cells overexpressing PD-YME1L1, levels of MNRR1 were again not reduced after LPS treatment (Figure 3D). Moreover, examination of a known substrate of YME1L1 proteolysis, STARD7 (MacVicar et al., 2019; Saita et al., 2018), showed LPS-stimulated reduction with active YME1L1 but not with PD-YME1L1 (Figure 3D). Thus, we conclude that MNRR1 levels are reduced in LPS-treated cells via the upstream protease YME1L1.

ATM kinase-mediated phosphorylation of YME1L1 enhances its stability

The finding that YME1L1 protein levels were increased in LPS-treated placental cells (Figure 3C) whereas transcript levels were unaffected (Figure S2A) suggested increased protein stability. We confirmed this finding by blocking new protein synthesis with cycloheximide, wherein YME1L1 showed increased stability after LPS treatment (Figure 4A). To uncover the basis of the increased stability, we hypothesized a protein modification and thus examined the post-translational profile of YME1L1. Upon treatment with LPS, YME1L1 protein in HTR cells displayed enhanced threonine phosphorylation (Figure 4B) but not serine or tyrosine phosphorylation (Figure S2D).

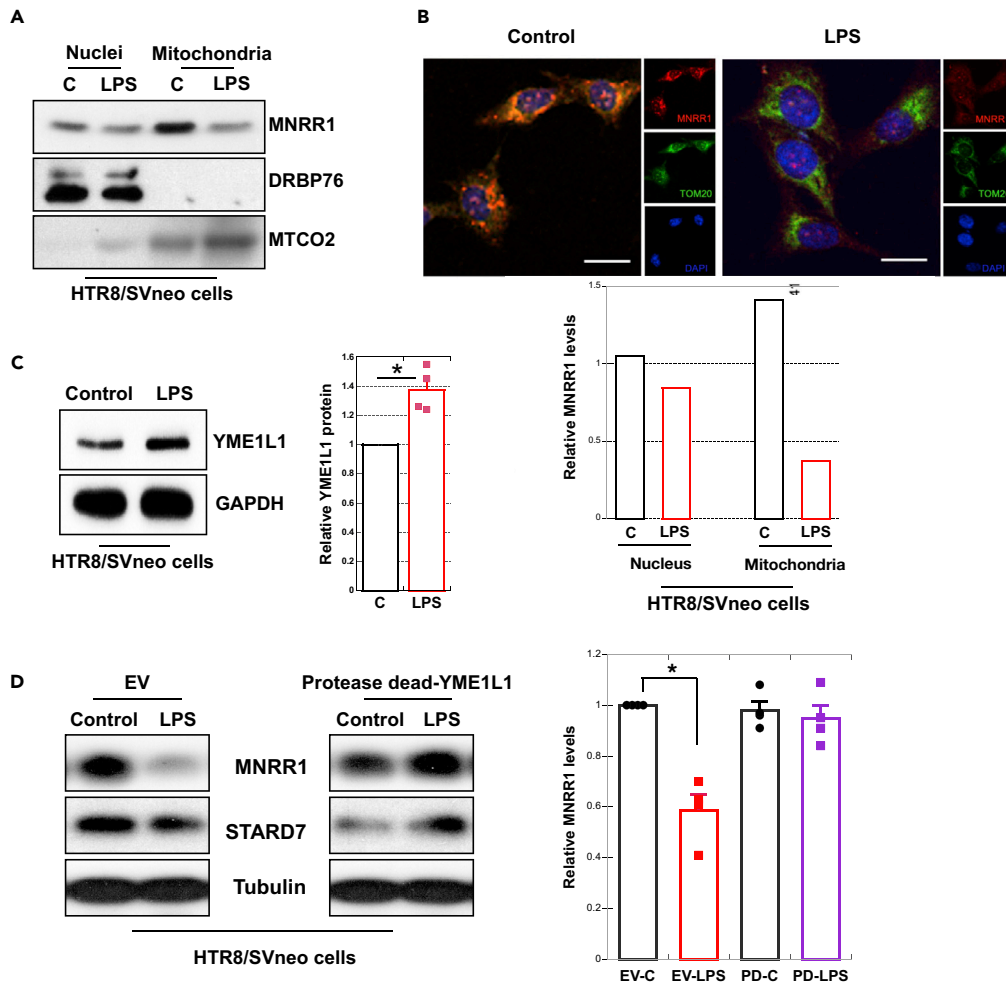


Figure 3. Compartment-specific reduction in MNRR1 levels in human placental cells treated with LPS is mediated by YME1L1 protease

(A) Equal amounts HTR cell nuclear and mitochondrial fractions were separated on an SDS-PAGE gel and probed for MNRR1. DRBP76 and MTCO2 were probed as nuclear and mitochondrial markers, respectively, to assess purity of fractions.

(B) HTR cells were treated with control (water) or LPS and immunostained for MNRR1 (red fluorescence). DAPI (blue fluorescence) was stained as a nuclear marker and TOM20 (green fluorescence) as a mitochondrial marker. Scale bar represents a distance of 20 μm . Below, the graph represents MNRR1 levels relative to a compartment-specific control for each treatment.

(C) *Left*, Equal amounts of HTR cells treated with control (water) or LPS were separated on an SDS-PAGE gel and probed for YME1L1. GAPDH was probed as a loading control. *Right*, the graph represents YME1L1 levels relative to GAPDH.

(D) *Left*, HTR cells overexpressing either an empty vector (EV) or a protease-dead (PD) mutant of YME1L1. Cells were treated with control (water) or LPS. Equal amounts of cell lysates were separated on an SDS-PAGE gel and probed for MNRR1 and STARD7. Tubulin was probed as a loading control. *Right*, the graph represents MNRR1 levels relative to Tubulin (n = 4 biological replicates).

To identify the threonine kinase for which YME1L1 is a substrate, we used Scansite (<https://scansite4.mit.edu/4.0/#home>), which identified ATM and NEK6 as candidate kinases for YME1L1 under high stringency conditions (Figure S3A). Of these, only ATM kinase interacted with YME1L1 in LPS-treated placental cells (Figure S3B) whereas NEK6 kinase did not (Figure S3C). To functionally assess this bioinformatic prediction, we utilized an inhibitor of ATM kinase activity and found that, when ATM kinase activity was inhibited, LPS-stimulated threonine phosphorylation of YME1L1 was blocked (Figure 4B). Concurrently, the reduction in levels of YME1L1 substrates MNRR1 and STARD7 was also blocked by the ATM inhibitor (Figure S3D). We next asked whether LPS-induced threonine phosphorylation of YME1L1 can affect the stability of the

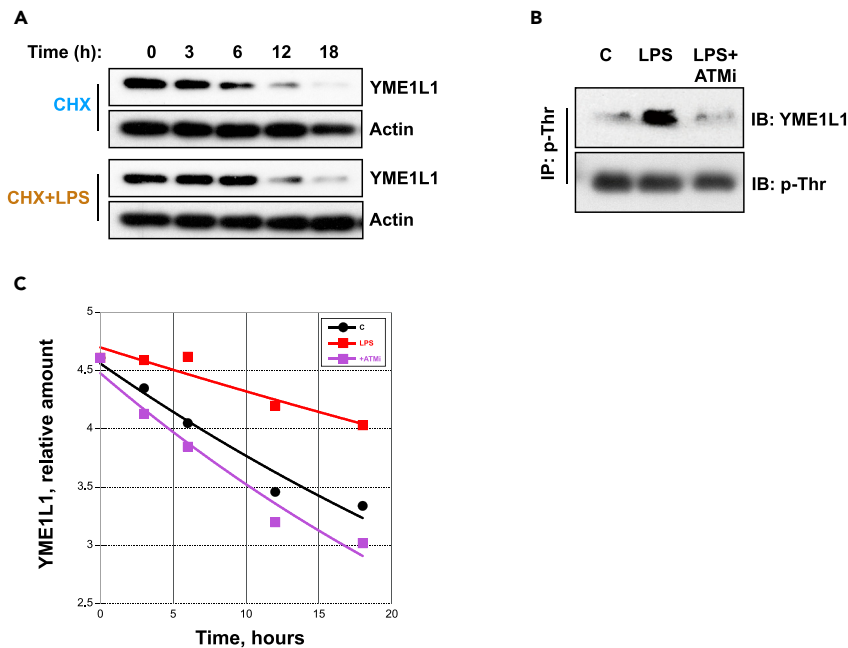


Figure 4. LPS treatment of placental cells increases the stability of YME1L1 via threonine phosphorylation by ATM kinase

(A) Equal numbers of HTR cells were plated on a 6-well plate and treated with control (water) or LPS and 100 $\mu\text{g}/\text{mL}$ cycloheximide for the durations shown. Equal amounts of cell lysates were separated on an SDS-PAGE gel and probed for YME1L1. Actin was probed as a loading control.

(B) HTR cells were treated with vehicle (water + DMSO), LPS (LPS + DMSO), or LPS plus ATM inhibitor (1 μM) for 24 h. Equal amounts of whole cell lysates were used for immunoprecipitation by phospho-threonine antibody. Equal amounts of IP eluates were probed for YME1L1 and heavy chain (p-Thr) was probed to assess loading.

(C) Graph for YME1L1 levels from HTR cells were treated with control (water), LPS, or LPS + ATM inhibitor (1 μM) and 100 $\mu\text{g}/\text{mL}$ cycloheximide for the durations shown in (A). The amount relative to time = 0 was graphed ($n = 2$ biological replicates).

protease. We found that YME1L1's half-life (8.1 h) is more than doubled by LPS treatment (22.0 h) and that this stabilization is lost when ATM kinase is inhibited (Figures 4C and S3E). These results suggest that YME1L1 stability is enhanced upon threonine phosphorylation by ATM kinase in LPS-treated placental cells, resulting in MNRR1 reduction and, consequently, downstream reduction in mitochondrial OCR (Figures 1A, 1D, and 1F), increased ROS levels (Figure 1C), and activation of pro-inflammatory signaling (Figure 1F). In summary, we show that MNRR1 reduction results from stabilization of YME1L1 protease upon phosphorylation by ATM kinase.

ROS generated by NOX2 activates ATM kinase in bacterial endotoxin-treated placental cells *in vitro*

To probe in more detail the upstream basis of ATM-induced YME1L1 stability, we noted a previously defined inflammatory pathway in which activation of ATM kinase by NOX2 was demonstrated (Wu et al., 2017). To determine whether this pathway was operating here, we first examined whether NOX2 increased in LPS-treated cells and found a robust increase (Figure 5A). We then inhibited NOX2 to ask whether doing so prevented the LPS-dependent reduction in MNRR1 levels and found that MNRR1 was stabilized by the NOX2 inhibitor GSK2795039 (Figure 5B).

If an activated NOX2-generated "ROS burst" is upstream of mitochondrial ROS (Kim et al., 2017), we hypothesized that we should be able to detect this before a peak in mitochondrially generated ROS. Indeed, following LPS treatment, we saw that total ROS peaks within 30 min (black bars) whereas mitochondrial ROS (red bars) peaks at about 16 h (Figure 5C). Furthermore, the increase seen in total ROS was blocked with a NOX2 inhibitor (gray bars), suggesting that the ROS generated by NOX2 can activate ATM kinase (Figure 5C). We tested ROS activation of ATM kinase in placental cells by treating cells with hydrogen peroxide. We again saw increased

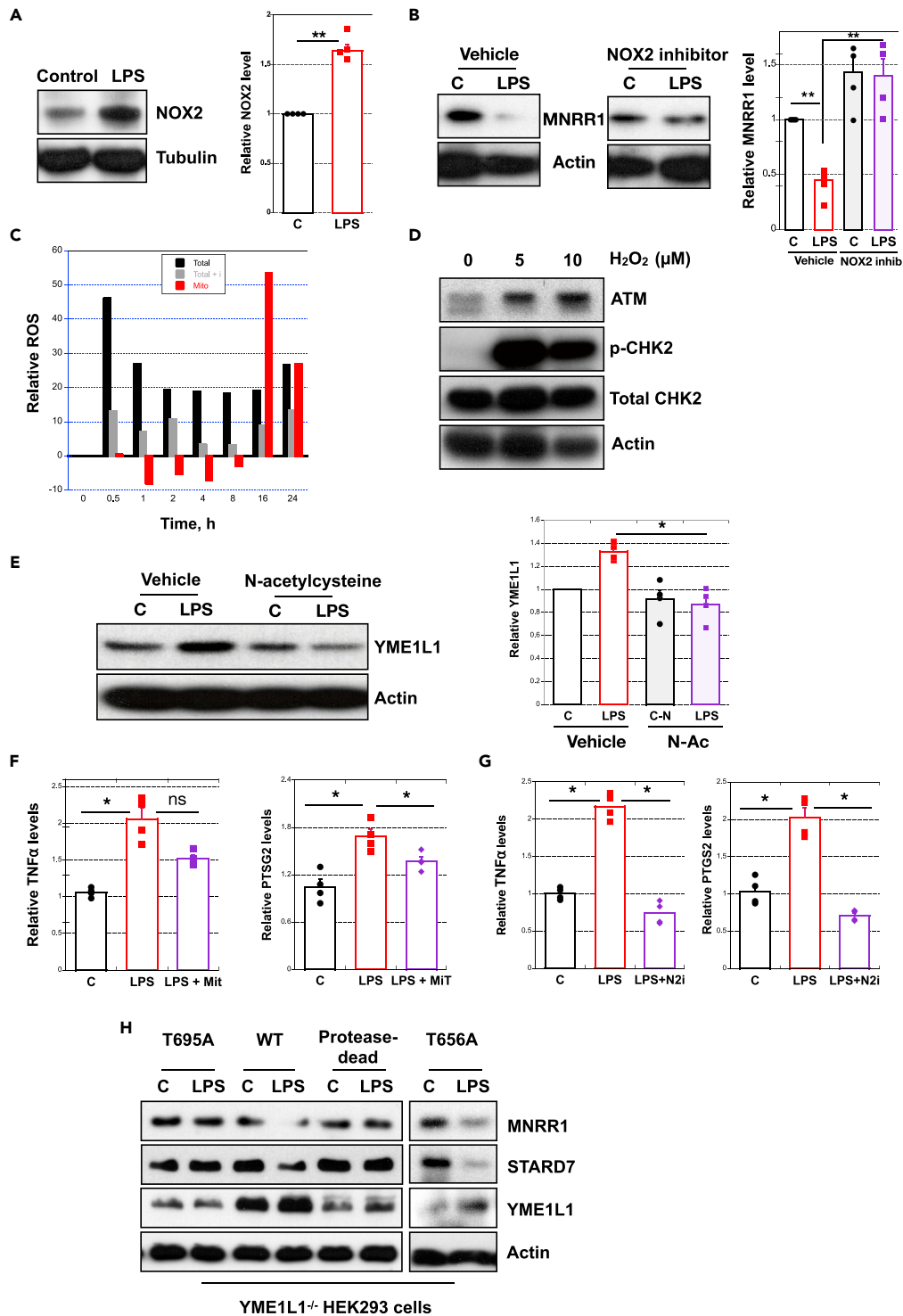


Figure 5. ROS generated by NOX2 activates ATM kinase in LPS-treated placental cells

(A–C) Left, Equal amounts of HTR cells treated with control (water) or LPS were separated on an SDS-PAGE gel and probed for NOX2. Tubulin was probed as a loading control. Right, NOX2 levels relative to tubulin are shown (n = 4 biological replicates). (B) Left, Equal amounts of HTR cells were treated for 24 h with control (water) or LPS and, for second blot, 25 μM NOX2 inhibitor (using DMSO in control); lysates were separated on an SDS-PAGE gel and probed for MNRR1. Actin was probed as a loading control. Right, Relative MNRR1 levels are shown for each lane (n = 4 biological replicates).

Figure 5. Continued

(C) HTR cells were treated with control (water) or LPS for the times shown, and ROS levels were measured as in Figure 1C. Total ROS, black; mitochondrial ROS, red; total ROS with ATM inhibitor, gray (n = 2 biological replicates). (D) Equal amounts of HTR cells were treated with control (water) or H₂O₂ for 16 h and lysates separated on an SDS-PAGE gel and probed for phospho-CHK2, total CHK2, and ATM kinase. Actin was probed as a loading control. (E) *Left*, Equal amounts of HTR cells treated with control (water) or LPS with either Vehicle (DMSO) or 100 μM N-acetyl cysteine for 24 h were separated on an SDS-PAGE gel and probed for YME1L1. Actin was probed as a loading control. *Right*, Relative YME1L1 levels are shown for each condition (n = 4 biological replicates). (F) *TNFα* and *PTGS2* transcript levels relative to *Actin* were measured in HTR cells treated with Control (water), LPS, or LPS +20 μM MitoTempo (n = 4 biological replicates). (G) *TNFα* and *PTGS2* relative transcript levels in HTR cells treated with Control (DMSO), LPS (LPS + DMSO) or LPS +25 μM NOX2 inhibitor (n = 4 biological replicates). (H) Equal amounts of YME1L1^{-/-} cells overexpressing WT or various mutants of YME1L1 were treated as control (water) or with LPS (1 μg/mL). Lysates were separated on an SDS-PAGE gel and probed for MNRR1, STARD7, and YME1L1. Actin was probed as a loading control.

ATM kinase as well as increased phosphorylation of a bona fide ATM kinase target CHK2 (Melchionna et al., 2000) (Figure 5D). We then tested the converse—whether scavenging ROS (with N-acetyl cysteine) would prevent LPS-stimulated phosphorylation of YME1L1 and found that such phosphorylation was indeed blocked (Figure 5E). Taken together, these data suggest that ATM kinase is activated by NOX2-generated ROS and can phosphorylate and thereby stabilize YME1L1, which in turn reduces MNRR1 levels.

To assess whether ROS-induced signaling was responsible for inflammation, we tested whether scavenging mitochondrial ROS or NOX2-mediated ROS would affect two markers of inflammation—*TNFα* (tumor necrosis factor alpha) and *PTGS2* (prostaglandin synthase 2; also, cyclooxygenase-2). We found that scavenging mitochondrial ROS (using MitoTempo, a mitochondria-specific ROS scavenger (Trnka et al., 2008) could partially reduce an LPS-induced increase in *TNFα* and *PTGS2* transcript levels (Figure 5F). The use of the NOX2 inhibitor, on the other hand, could completely protect the increase in the same markers (Figure 5G), suggesting that mitochondrial ROS is downstream of the NOX2-induced cytoplasmic ROS and that scavenging mitochondrial ROS only partially inhibits inflammation.

To further define the role of YME1L1 phosphorylation, we generated a non-phosphorylatable point mutation (T695A) at the predicted target, threonine 695 (Figure S3A). We tested the effect of this mutation in YME1L1-KO 293, the only available model to study these effects since a knockout of YME1L1 in mice post-implantation of the embryo is lethal (Wai et al., 2015). Hence, we used YME1L1-KO HEK293 cells and overexpressed this T695A mutant, WT, or PD-YME1L1 to rule out the effect of any endogenous YME1L1. Doing so, we found that the T695A mutation prevented the LPS-stimulated reduction in MNRR1 levels that is seen when the WT form is present, suggesting this phosphorylation is necessary for LPS-induced stabilization of YME1L1. Furthermore, this mutation behaves like PD-YME1L1 with respect to its known substrate STARD7 (Figure 5H). The T695A mutation thus acts in a similar manner to PD-YME1L1. A second, control mutation, T656A, at a different threonine residue with a canonical ATM kinase recognition motif (Pines et al., 2011), does not prevent LPS-stimulated MNRR1 reduction (Figure 5H), supporting the specificity of the T695 phosphorylation site in response to LPS treatment.

A TLR4-independent signaling pathway is responsible for MNRR1-dependent reduction in mitochondrial function in bacterial endotoxin-treated placental cells *in vitro*

Canonical LPS signaling is initiated by binding to Toll-like receptor 4 (TLR4) (Hoshino et al., 1999; Poltorak et al., 1998); therefore, we next asked if overexpression of TLR4 activates the NOX2-ATM-MNRR1 signaling pathway. We found that, although overexpression of TLR4 increases MNRR1 levels, LPS treatment reduces MNRR1 similarly to control cells (Figure S4A). Since inflammation caused by LPS can occur either through MyD88-dependent signaling or MyD88-independent (TBK1-dependent) signaling (Kawai and Akira, 2011), we next asked whether MNRR1 levels are reduced in WT or Myd88^{-/-} mice challenged with LPS. We found that MNRR1 levels are reduced in both WT and Myd88^{-/-} mice (Figure S4B). Furthermore, examining activation of the kinase promoting the MyD88-independent immune response, we also found no change in TBK1 phosphorylation in HTR placental cells (Figure S4C). Taken together, these results eliminate the canonical TLR4 signaling pathway as the mediator of mitochondrial dysfunction in placental cells.

We then hypothesized that TLR4 may directly interact with NOX2 to initiate this pathway, and hence tested MNRR1 levels in TLR4^{-/-} tissue lysates from mice injected with PBS (control) or LPS. We found that MNRR1

levels are reduced also in TLR4^{-/-} mouse livers challenged with LPS (Figure S4D). Besides MNRR1, we tested for other markers (NOX2 and ATM kinase) both in the LPS-injected mouse placentas (Figure S4E), where we originally found a reduction in MNRR1 (Figure 2A), as well as in the TLR4^{-/-} mouse tissue lysates (data not shown). We found the pathway to be active even in the animal samples, consistent with the results found in the human cell culture system (Figure S4C and 5A). To verify that the TLR4-independent reduction in MNRR1 levels seen in the TLR4^{-/-} animals is initiated by NOX2 activation, we used a NOX2 inhibitor in TLR4^{-/-} mouse macrophages (Andrade et al., 2016) and found that the NOX2 inhibitor prevents LPS-induced reduction in MNRR1 (data not shown). Taken together, we conclude that LPS acts through a TLR4-independent pathway to activate ATM kinase to phosphorylate YME1L1 at Thr-695, stabilizing it and thereby reducing MNRR1 levels.

MNRR1 functions as an anti-inflammatory effector via its nuclear function

To confirm that MNRR1 is upstream of the inflammatory signaling, we generated a MNRR1-depleted human placental cell line and assessed levels of two inflammatory markers—JNK phosphorylation (Figure S5A) and transcript levels of *TNF α* (Figure S5B)—and found these to be increased. Since MNRR1 is present in both the nucleus and the mitochondria and has a different function in each (Aras et al., 2015), we investigated the compartment-specific effect of LPS on MNRR1 by assessing OCR and the stimulation of inflammation-associated genes *TNF α* and *PTGS2*. We found that LPS treatment increased the transcript levels of both these genes and that overexpression of either WT or the C-S mutant of MNRR1, which does not localize to mitochondria (Aras et al., 2015), can prevent this increase (Figures 6A and 6B), as can the MNRR1 activator nitazoxanide (N) (Figures 6C and 6D). To further explore whether the anti-inflammatory role is due to nuclear function of MNRR1, we asked if overexpressing CHCHD4 (MIA40), which is required for MNRR1 import into the mitochondria (Aras et al., 2015), could prevent the LPS-induced deficit in oxygen consumption. We found that CHCHD4 overexpression can increase oxygen consumption (Figure S5C), as also shown previously (Yang et al., 2012), but that LPS treatment reduces oxygen consumption to the same extent as seen in the absence of CHCHD4 overexpression, suggesting that specifically nuclear MNRR1 is required to prevent inflammation.

To probe the mechanism by which nuclear MNRR1 can inhibit inflammation, we examined whether any regulatory components of the NF- κ B signaling pathway are transcriptionally regulated by MNRR1. We previously found that I- κ B α (*NFKBIA*), a regulator that binds NF- κ B and retains it in the cytoplasm (Haskill et al., 1991), is transcriptionally activated by MNRR1 (Aras et al., 2019). We confirmed this in the placental cells by measuring transcript levels of *NFKBIA*. These were reduced in KO cells (Figure 6E; compare bars 1 and 2) and rescued using the transcriptionally active version of MNRR1 cells (compare bars 2 and 3). Consistent with the transcript levels, we also found in the placental cells that I- κ B α levels are reduced by LPS treatment (Figure 6F), thereby allowing nuclear localization of NF- κ B. Overexpression of MNRR1, however, can prevent these effects (Figure 6F), suggesting that MNRR1 can act as an anti-inflammatory agent at least in part by preventing activation of NF- κ B. Since one of the classic targets of NF- κ B, cyclooxygenase-2, is required for induction of labor under physiological conditions (Bennett and Slater, 1996; Olson and Ammann, 2007), MNRR1 expression may blunt the effects of inflammation by preventing nuclear translocation of NF- κ B.

DISCUSSION

Mitochondria are known to serve as an early sensor of inflammatory stress (Lang et al., 1988; Tiku et al., 2020; Vringer and Tait, 2019; Zhong et al., 2019). Here, we show that MNRR1 is reduced by a post-translational mechanism in both *in vivo* and *in vitro* models of placental inflammation, leading to the generation of mitochondrial ROS. Surprisingly, the mitochondrial ROS that is the source of inflammatory signaling in the placenta takes place via a TLR4-independent signaling pathway. This pathway is initiated by activation of ATM kinase via NOX2-dependent ROS, which in turn phosphorylates YME1L1, a protease that degrades MNRR1 in the mitochondria. Although ATM kinase is primarily activated in response to DNA damage (Lee and Paull, 2007), it was also shown to be activated in response to LPS treatment in macrophage cells (Weintz et al., 2010) although the downstream signaling targets were not identified. A recent study in a renal tubular epithelial cell model of LPS-induced sepsis (Zheng et al., 2019) also identifies ATM activation as playing a key role in inflammation and autophagy activation. ATM kinase is localized to mitochondria (Valentin-Vega et al., 2012), more specifically to the inner mitochondrial membrane (Blignaut et al., 2019), the same sub-mitochondrial compartment that harbors YME1L1. Although YME1L1 is embedded in the inner membrane, a large catalytic domain is exposed

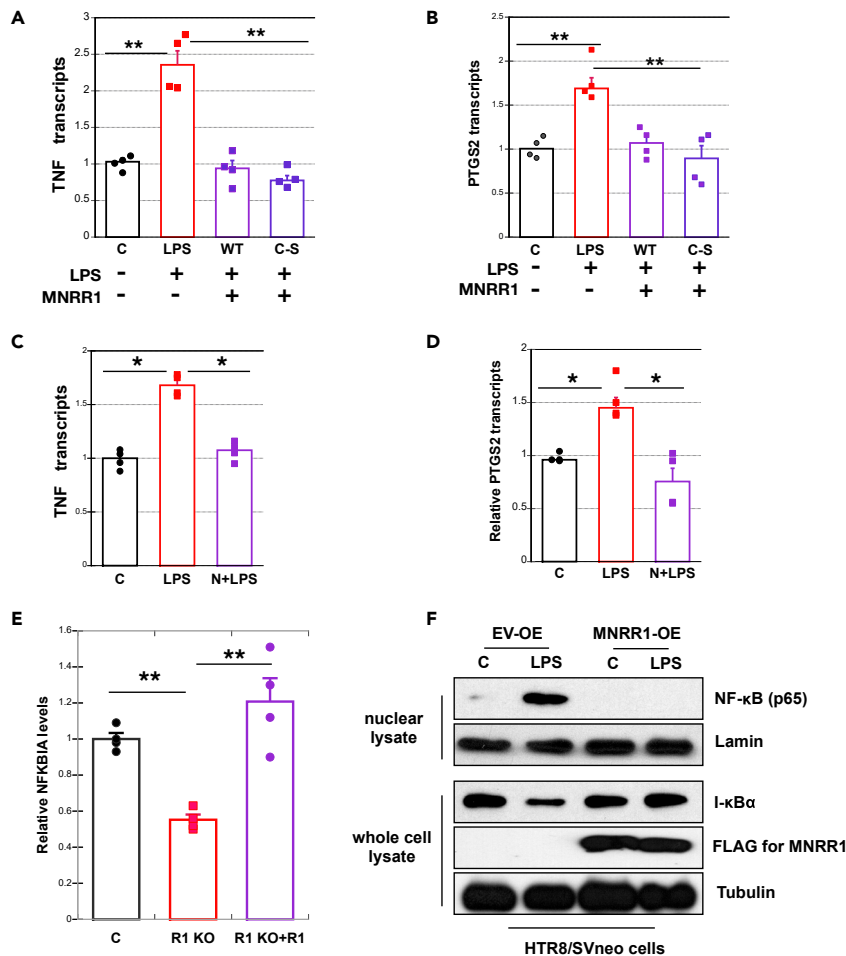


Figure 6. MNRR1 functions as anti-inflammatory via its nuclear function

(A and B) Relative *TNFα* (A) and *PTGS2* (B) transcript levels in HTR cells treated with Control (EV, empty vector), LPS (EV + LPS), WT-MNRR1 (WT + LPS), or C-S-MNRR1 (C-S + LPS). (n = 4 biological replicates).

(C and D) Relative *TNFα* and (D) *PTGS2* transcript levels in HTR cells treated with Control (DMSO), LPS (LPS + DMSO), or LPS + 10 μM Nitazoxanide (N). (n = 4 biological replicates).

(E) Transcript levels for *NFKB1A* are significantly reduced in HTR MNRR1-knockout cells (KO) relative to wild type controls (WT). This reduction is rescued by overexpressing the transcriptionally active mutant of MNRR1 (K119R-MNRR1) in MNRR1-KO (n = 4 biological replicates).

(F) *Nuclear lysate*: NF-κB levels from cells containing overexpressed (OE) EV (empty vector) or MNRR1, each treated or not with LPS. Lamin was probed as a nuclear loading control. *Whole cell lysate*: Cells were from the same experiment and total lysates were probed for I-κB and FLAG (MNRR1) levels. Tubulin was probed as a loading control.

that faces the IMS (Leonhard et al., 1996). We have shown that ATM-mediated threonine phosphorylation of YME1L1 can enhance its stability, resulting in faster turnover of MNRR1 in the mitochondria. Depletion of MNRR1 results in reduced oxygen consumption, reduced ATP levels, and increased ROS. These changes activate a self-amplifying inflammatory signaling cascade that may disrupt signaling at the fetal-maternal interface.

MNRR1 has previously been associated with several diseases both in terms of altered expression and through mutations. Depleted MNRR1 protein levels have been found in an *in vivo* model for juvenile Niemann Pick type C disease (Erickson et al., 2020) and in an *in vitro* model for MELAS (mitochondrial encephalomyopathy lactic acidosis and stroke-like episodes) syndrome (Aras et al., 2020). Mutations in MNRR1 have been associated with a number of neurodegenerative diseases such as Parkinson's disease, Alzheimer's disease, and Charcot-Marie-Tooth type 1A (Grossman et al., 2017). Of note, MELAS, caused by a mtDNA mutation in the mitochondrial tRNA^{Leu(UUR)} gene (m.3243A > G), has been associated

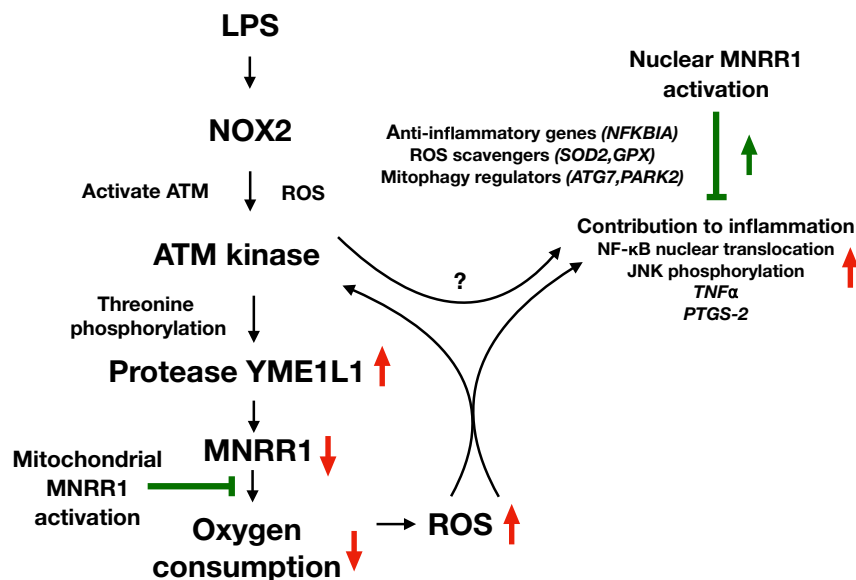


Figure 7. Model of MNRR1 action to suppress inflammation

Schematic summary of the role of MNRR1 in inflammation. Bacterial endotoxin activates ATM kinase via NOX2-mediated ROS. Increased ATM activity in turn stabilizes YME1L1 protease by enhancing its threonine phosphorylation. Increased YME1L1 protease degrades MNRR1 to reduce oxygen consumption and increase ROS levels, which contribute to inflammation evidenced by increased levels of *TNFα* and cyclooxygenase-2 (*PTGS2*). Activation of MNRR1 can prevent a reduction in mitochondrial function and increase of ROS levels, thereby preventing inflammation.

with spontaneous preterm birth (de Laat et al., 2015; Feeney et al., 2019) and increased incidence of pre-eclampsia and gestational diabetes mellitus (de Laat et al., 2015). We have recently shown that increased expression of MNRR1 can rescue the oxygen consumption and other deficits associated with MELAS *in vitro* (Aras et al., 2020). MNRR1 activation, either by overexpression or, perhaps more usefully, with a chemical activator, can thus provide multiple benefits that protect placental mitochondria and reduce inflammation.

MNRR1 is known to function in both the nucleus and the mitochondria (Aras et al., 2013, 2015, 2017; Purandare et al., 2018), and as a nuclear transactivator can promote its own transcription (Aras et al., 2015). Although we have focused here on the consequences of mitochondrial depletion, the rescue by pharmacological activation of transcription (Figure 1F) and by overexpression of MNRR1 that cannot enter the mitochondria (Figures 6A and 6B) suggests that activating its nuclear function could suffice to prevent placental damage. In addition to activating itself, MNRR1 is a transcriptional activator for ROS scavenging enzymes such as *SOD2* (superoxide dismutase) and *GPX* (glutathione peroxidase) (Aras et al., 2015) and also is a regulator of mitophagy genes such as *ATG7* and *PARK2* (Parkin) (Aras et al., 2020). A similar conclusion about the importance of its nuclear function was reached in a MELAS model (Aras et al., 2020). Besides MNRR1's ability to regulate genes involved in ROS scavenging, we now identify at least one other transcriptional target—*IkBα*—that can contribute to its anti-inflammatory role via inhibition of NF- κ B.

The novel NOX2/ATM kinase/YME1L1/MNRR1/cyclooxygenase-2 axis we have described provides insight into the mechanism by which placental inflammation can lead to preterm labor and birth (Figure 7). There are multiple points at which we could modulate this pathway; yet we consider activation of MNRR1 may be an ideal point to break the cycle of ROS-induced inflammation. Cyclooxygenase-2 was initially considered an ideal target since its pharmacological inhibition can prevent inflammation-induced preterm labor (Gross et al., 2000) in mice. Another current treatment uses steroidal compounds in the antenatal period to prevent respiratory distress syndrome and mortality in anticipated cases of preterm birth (Briceno-Perez et al., 2019). However, steroids are not always useful and have been associated with deleterious effects both on the fetus such as cerebral palsy (Wapner et al., 2007), microcephaly (Carson et al., 2016), lower birthweight (Bloom et al., 2001), adrenal suppression (Banks et al., 1999), the development of impaired glucose

tolerance and hypertension later in life (Seckl et al., 2000), and on the mother, such as risk of infection (Abbasi et al., 2000), loss of glycemic control in diabetics (Battarbee et al., 2019), suppression of the hypothalamic axis (McKenna et al., 2000), and reduced fetal growth velocity (Rizzo et al., 2020). Since the pro-inflammatory signaling proceeds through degradation of mitochondrial MNRR1 whereas its nuclear function is sufficient to rescue the effects of LPS, a transcriptional activator of MNRR1 may provide another treatment option. In addition, the recent demonstration that MNRR1 activation may be able to augment or in some cases even replace steroids for respiratory distress syndrome (Purandare et al., 2021) adds additional impetus for development of this targeted therapy.

In summary, we have identified a novel signaling axis by which inflammation induced by the bacterial LPS causes mitochondrial dysfunction. It does so by reducing the level of the bi-organellar regulator MNRR1 in response to phosphorylation and stabilization of the IMS protease YME1L1, which turns over MNRR1. Phosphorylation is carried out by ATM kinase after activation by NOX2-produced ROS promoted by LPS. The mitochondrial ROS that stems from MNRR1 inhibition causes JNK phosphorylation and consequent activation of the cytokines TNF α and cyclooxygenase-2. The ubiquitous nature of MNRR1 depletion due to inflammation found in multiple cell lines suggests that MNRR1 is an important target integral to the mitochondrial dysfunction due to inflammation. Furthermore, given its bi-organellar role, activation of MNRR1 can be used to rescue mitochondrial deficits seen under conditions of inflammation in the placenta, as we show here, and possibly other tissues affected by inflammation.

Limitations of this study

A limitation of this study is that we have used placental cell lines and a mouse model to dissect the novel pathway we are reporting. Although doing so allowed the mechanistic studies, it remains to be seen how well the results are recapitulated in human subjects. In addition, we have used lipopolysaccharide from *Escherichia coli* to produce the inflammation we studied whereas intact organisms often induce placental inflammation. Thus, the generality of the response to LPS needs to be determined.

STAR★METHODS

Detailed methods are provided in the online version of this paper and include the following:

- KEY RESOURCES TABLE
- RESOURCE AVAILABILITY
 - Lead contact
 - Materials availability
 - Data and code availability
- METHODS DETAILS
 - Cell culture and reagents
 - Transient transfection of HTR cells
 - Real-time PCR
 - Luciferase reporter assay
 - Intact cellular oxygen consumption
 - ATP measurements
 - ROS measurements
 - Confocal microscopy
 - Mitochondria isolation
 - Immunoblotting and co-immunoprecipitation
 - Animal experiments and injections
- QUANTIFICATION AND STATISTICAL ANALYSIS

SUPPLEMENTAL INFORMATION

Supplemental information can be found online at <https://doi.org/10.1016/j.isci.2022.105342>.

ACKNOWLEDGMENTS

We thank Dr. Thomas Langer (University of Cologne, Cologne, Germany) for providing the YME1L1 plasmids, Dr. Kezhong Zhang (Wayne State University, Detroit, MI, USA) for providing the MyD88^{-/-} tissues and TLR4^{-/-} tissue lysates, and Dr. Douglas Golenbock (University of Massachusetts Medical School,

Worcester, MA, USA) for providing the TLR4^{+/+} and TLR4^{-/-} mouse macrophages. This work was supported by the Perinatology Research Branch, Division of Obstetrics and Maternal-Fetal Medicine, Division of Intramural Research, Eunice Kennedy Shriver National Institute of Child Health and Human Development, National Institutes of Health, U.S. Department of Health and Human Services (NICHD/NIH/DHHS); and, in part, with Federal funds from NICHD/NIH/DHHS under Contract No. HHSN275201300006C. Dr. Romero has contributed to this work as part of his official duties as an employee of the United States Federal Government. Opinions, interpretations, conclusions, and recommendations are those of the authors and are not necessarily endorsed by the NIH.

AUTHOR CONTRIBUTIONS

N.P. performed all experiments, Y.K. helped with generation of Western blots, R.R. and N.G.L. provided the human and mouse placental tissue samples, and provided intellectual feedback. N.P., S.A., and L.I.G. analyzed the results and participated in experimental design. Y.X. and A.F. performed the screen to identify MNRR1 activators and inhibitors. N.P. and L.I.G. wrote the manuscript. All authors reviewed the manuscript.

DECLARATION OF INTERESTS

The authors declare that they have no competing interests.

Received: November 22, 2021

Revised: June 20, 2022

Accepted: October 10, 2022

Published: November 18, 2022

REFERENCES

- Abbasi, S., Hirsch, D., Davis, J., Tolosa, J., Stouffer, N., Debbs, R., and Gerdes, J.S. (2000). Effect of single versus multiple courses of antenatal corticosteroids on maternal and neonatal outcome. *Am. J. Obstet. Gynecol.* **182**, 1243–1249.
- Andrade, W.A., Agarwal, S., Mo, S., Shaffer, S.A., Dillard, J.P., Schmidt, T., Hornung, V., Fitzgerald, K.A., Kurt-Jones, E.A., and Golenbock, D.T. (2016). Type I interferon induction by *Neisseria gonorrhoeae*: dual requirement of cyclic GMP-AMP synthase and toll-like receptor 4. *Cell Rep.* **15**, 2438–2448. <https://doi.org/10.1016/j.celrep.2016.05.030>.
- Aras, S., Arrabi, H., Purandare, N., Huttemann, M., Kamholz, J., Zuchner, S., and Grossman, L.I. (2017). Abl2 kinase phosphorylates Bi-organellar regulator MNRR1 in mitochondria, stimulating respiration. *Biochim. Biophys. Acta Mol. Cell Res.* **1864**, 440–448. <https://doi.org/10.1016/j.bbamcr.2016.11.029>.
- Aras, S., Bai, M., Lee, I., Springett, R., Huttemann, M., and Grossman, L.I. (2015). MNRR1 (formerly CHCHD2) is a bi-organellar regulator of mitochondrial metabolism. *Mitochondrion* **20**, 43–51. <https://doi.org/10.1016/j.mito.2014.10.003>.
- Aras, S., Maroun, M.C., Song, Y., Bandyopadhyay, S., Stark, A., Yang, Z.Q., Long, M.P., Grossman, L.I., and Fernandez-Madrid, F. (2019). Mitochondrial autoimmunity and MNRR1 in breast carcinogenesis. *BMC Cancer* **19**, 411. <https://doi.org/10.1186/s12885-019-5575-7>.
- Aras, S., Pak, O., Sommer, N., Finley, R., Jr., Huttemann, M., Weissmann, N., and Grossman, L.I. (2013). Oxygen-dependent expression of cytochrome c oxidase subunit 4-2 gene expression is mediated by transcription factors RBPJ, CXXC5 and CHCHD2. *Nucleic Acids Res.* **41**, 2255–2266. <https://doi.org/10.1093/nar/gks1454>.
- Aras, S., Purandare, N., Gladys, S., Somayajulu-Nitu, M., Zhang, K., Wallace, D.C., and Grossman, L.I. (2020). Mitochondrial Nuclear Retrograde Regulator 1 (MNRR1) rescues the cellular phenotype of MELAS by inducing homeostatic mechanisms. *Proc. Natl. Acad. Sci. USA* **117**, 32056–32065. <https://doi.org/10.1073/pnas.2005877117>.
- Banks, B.A., Cnaan, A., Morgan, M.A., Parer, J.T., Merrill, J.D., Ballard, P.L., and Ballard, R.A. (1999). Multiple courses of antenatal corticosteroids and outcome of premature neonates. *North American Thyrotropin-Releasing Hormone Study Group. Am. J. Obstet. Gynecol.* **181**, 709–717.
- Battarbee, A.N., Aliaga, S., and Boggess, K.A. (2019). Management of diabetic women with threatened preterm birth: a survey of Maternal-Fetal Medicine providers. *J. Matern. Fetal Neonatal Med.* **1–9**. <https://doi.org/10.1080/14767058.2019.1566307>.
- Bennett, P., and Slater, D. (1996). COX-2 expression in labour. In *Improved non-steroid anti-inflammatory drugs: COX-2 enzyme inhibitors* (Springer), pp. 167–188.
- Blignaut, M., Loos, B., Botchway, S.W., Parker, A.W., and Huisamen, B. (2019). Ataxia-Telangiectasia Mutated is located in cardiac mitochondria and impacts oxidative phosphorylation. *Sci. Rep.* **9**, 4782. <https://doi.org/10.1038/s41598-019-41108-1>.
- Bloom, S.L., Sheffield, J.S., McIntire, D.D., and Leveno, K.J. (2001). Antenatal dexamethasone and decreased birth weight. *Obstet. Gynecol.* **97**, 485–490.
- Briceno-Perez, C., Reyna-Villasmiel, E., and Vigil-De-Gracia, P. (2019). Antenatal corticosteroid therapy: historical and scientific basis to improve preterm birth management. *Eur. J. Obstet. Gynecol. Reprod. Biol.* **234**, 32–37. <https://doi.org/10.1016/j.ejogrb.2018.12.025>.
- Carson, R., Monaghan-Nichols, A.P., DeFranco, D.B., and Rudine, A.C. (2016). Effects of antenatal glucocorticoids on the developing brain. *Steroids* **114**, 25–32. <https://doi.org/10.1016/j.steroids.2016.05.012>.
- Dandekar, A., Qiu, Y., Kim, H., Wang, J., Hou, X., Zhang, X., Zheng, Z., Mendez, R., Yu, F.S., Kumar, A., et al. (2016). Toll-like receptor (TLR) signaling interacts with CREBH to modulate high-density lipoprotein (HDL) in response to bacterial endotoxin. *J. Biol. Chem.* **291**, 23149–23158. <https://doi.org/10.1074/jbc.M116.755728>.
- de Laat, P., Fleuren, L.H., Bekker, M.N., Smeitink, J.A., and Janssen, M.C. (2015). Obstetric complications in carriers of the m.3243A>G mutation, a retrospective cohort study on maternal and fetal outcome. *Mitochondrion* **25**, 98–103. <https://doi.org/10.1016/j.mito.2015.10.005>.
- Erickson, R.P., Aras, S., Purandare, N., Huttemann, M., Liu, J., Dragotto, J., Fiorenza, M.T., and Grossman, L.I. (2020). Decreased membrane cholesterol in liver mitochondria of the point mutation mouse model of juvenile Niemann-Pick C1, *Npc1*(nmf164). *Mitochondrion* **51**, 15–21. <https://doi.org/10.1016/j.mito.2019.12.003>.
- Feeney, C.L., Lim, A.Z., Fagan, E., Blain, A., Bright, A., Maddison, J., Devine, H., Stewart, J., Taylor, R.W., Gorman, G.S., et al. (2019). A case-comparison study of pregnant women with mitochondrial disease - what to expect? *BJOG*

126, 1380–1389. <https://doi.org/10.1111/1471-0528.15667>.

Gomez-Lopez, N., Motomura, K., Miller, D., Garcia-Flores, V., Galaz, J., and Romero, R. (2019). Inflammasomes: their role in normal and complicated pregnancies. *J. Immunol.* 203, 2757–2769. <https://doi.org/10.4049/jimmunol.1900901>.

Gomez-Lopez, N., Romero, R., Arenas-Hernandez, M., Panaitescu, B., Garcia-Flores, V., Mial, T.N., Sahi, A., and Hassan, S.S. (2018). Intra-amniotic administration of lipopolysaccharide induces spontaneous preterm labor and birth in the absence of a body temperature change. *J. Matern. Fetal Neonatal Med.* 31, 439–446. <https://doi.org/10.1080/14767058.2017.1287894>.

Gross, G., Imamura, T., Vogt, S.K., Wozniak, D.F., Nelson, D.M., Sadovsky, Y., and Muglia, L.J. (2000). Inhibition of cyclooxygenase-2 prevents inflammation-mediated preterm labor in the mouse. *Am. J. Physiol. Regul. Integr. Comp. Physiol.* 278, R1415–R1423. <https://doi.org/10.1152/ajpregu.2000.278.6.R1415>.

Grossman, L.I., Purandare, N., Arshad, R., Gladys, S., Somayajulu, M., Huttemann, M., and Aras, S. (2017). MNRR1, a biorganellar regulator of mitochondria. *Oxid. Med. Cell. Longev.* 2017, 6739236. <https://doi.org/10.1155/2017/6739236>.

Haskill, S., Beg, A.A., Tompkins, S.M., Morris, J.S., Yurochko, A.D., Sampson-Johannes, A., Mondal, K., Ralph, P., and Baldwin, A.S., Jr. (1991). Characterization of an immediate-early gene induced in adherent monocytes that encodes I kappa B-like activity. *Cell* 65, 1281–1289. [https://doi.org/10.1016/0092-8674\(91\)90022-q](https://doi.org/10.1016/0092-8674(91)90022-q).

Holland, O.J., Hickey, A.J.R., Alvsaker, A., Moran, S., Hedges, C., Chamley, L.W., and Perkins, A.V. (2017). Changes in mitochondrial respiration in the human placenta over gestation. *Placenta* 57, 102–112. <https://doi.org/10.1016/j.placenta.2017.06.011>.

Hoshino, K., Takeuchi, O., Kawai, T., Sanjo, H., Ogawa, T., Takeda, Y., Takeda, K., and Akira, S. (1999). Cutting edge: toll-like receptor 4 (TLR4)-deficient mice are hyporesponsive to lipopolysaccharide: evidence for TLR4 as the Lps gene product. *J. Immunol.* 162, 3749–3752.

Kawai, T., and Akira, S. (2011). Toll-like receptors and their crosstalk with other innate receptors in infection and immunity. *Immunity* 34, 637–650. <https://doi.org/10.1016/j.immuni.2011.05.006>.

Kim, Y.M., Kim, S.J., Tatsunami, R., Yamamura, H., Fukui, T., and Ushio-Fukai, M. (2017). ROS-induced ROS release orchestrated by Nox4, Nox2, and mitochondria in VEGF signaling and angiogenesis. *Am. J. Physiol. Cell Physiol.* 312, C749–C764. <https://doi.org/10.1152/ajpcell.00346.2016>.

Lang, R.M., Borow, K.M., Neumann, A., Carroll, J.D., Weinert, L., Murphy, M.B., Ghali, J., and Rajfer, S.I. (1988). Role of the beta 2 adrenoceptor in mediating positive inotropic activity in the failing heart and its relation to the hemodynamic actions of dopexamine hydrochloride. *Am. J. Cardiol.* 62, 46C–52C. [https://doi.org/10.1016/s0002-9149\(88\)80067-5](https://doi.org/10.1016/s0002-9149(88)80067-5).

Lee, J.H., and Paull, T.T. (2007). Activation and regulation of ATM kinase activity in response to

DNA double-strand breaks. *Oncogene* 26, 7741–7748. <https://doi.org/10.1038/sj.onc.1210872>.

Leonhard, K., Herrmann, J.M., Stuart, R.A., Mannhaupt, G., Neupert, W., and Langer, T. (1996). AAA proteases with catalytic sites on opposite membrane surfaces comprise a proteolytic system for the ATP-dependent degradation of inner membrane proteins in mitochondria. *EMBO J.* 15, 4218–4229.

Liu, Y., Clegg, H.V., Leslie, P.L., Di, J., Tollini, L.A., He, Y., Kim, T.H., Jin, A., Graves, L.M., Zheng, J., and Zhang, Y. (2015). CHCHD2 inhibits apoptosis by interacting with Bcl-x L to regulate Bax activation. *Cell Death Differ.* 22, 1035–1046. <https://doi.org/10.1038/cdd.2014.194>.

Liu, Y.T., Huang, X., Nguyen, D., Shammas, M.K., Wu, B.P., Dombi, E., Springer, D.A., Poulton, J., Sekine, S., and Narendra, D.P. (2020). Loss of CHCHD2 and CHCHD10 activates OMA1 peptidase to disrupt mitochondrial cristae phenocopying patient mutations. *Hum. Mol. Genet.* 29, 1547–1567. <https://doi.org/10.1093/hmg/ddaa077>.

MacVicar, T., Ohba, Y., Nolte, H., Mayer, F.C., Tatsuta, T., Sprenger, H.G., Lindner, B., Zhao, Y., Li, J., Bruns, C., et al. (2019). Lipid signalling drives proteolytic rewiring of mitochondria by YME1L. *Nature* 575, 361–365. <https://doi.org/10.1038/s41586-019-1738-6>.

Madrid, F.F., Grossman, L.I., and Aras, S. (2020). Mitochondria autoimmunity and MNRR1 in breast carcinogenesis: a review. *J. Cancer Immunol (Wilmington)* 2, 138–158. <https://doi.org/10.33696/cancerimmunol.2.027>.

Mando, C., Marino, M.A., Miriam, F., Palma, C.D., Borelli, M., Trabattini, D., Stampalija, T., Ferrazzi, E., Clementi, E., and Cetin, I. (2012). OS048 Mitochondrial content and function in placental cells and tissues of preeclampsia and IUGR. *Pregnancy Hypertens* 2, 203. <https://doi.org/10.1016/j.preghy.2012.04.049>.

McKenna, D.S., Wittber, G.M., Nagaraja, H.N., and Samuels, P. (2000). The effects of repeat doses of antenatal corticosteroids on maternal adrenal function. *Am. J. Obstet. Gynecol.* 183, 669–673. <https://doi.org/10.1067/mob.2000.106755>.

Melchionna, R., Chen, X.B., Blasina, A., and McGowan, C.H. (2000). Threonine 68 is required for radiation-induced phosphorylation and activation of Cds1. *Nat. Cell Biol.* 2, 762–765. <https://doi.org/10.1038/35036406>.

Mele, J., Muralimanoharan, S., Maloyan, A., and Myatt, L. (2014). Impaired mitochondrial function in human placenta with increased maternal adiposity. *Am. J. Physiol. Endocrinol. Metab.* 307, E419–E425. <https://doi.org/10.1152/ajpendo.00025.2014>.

Muralimanoharan, S., Maloyan, A., Mele, J., Guo, C., Myatt, L.G., and Myatt, L. (2012). MIR-210 modulates mitochondrial respiration in placenta with preeclampsia. *Placenta* 33, 816–823. <https://doi.org/10.1016/j.placenta.2012.07.002>.

Oh, K.J., Kim, S.M., Hong, J.S., Maymon, E., Erez, O., Panaitescu, B., Gomez-Lopez, N., Romero, R., and Yoon, B.H. (2017). Twenty-four percent of patients with clinical chorioamnionitis in preterm gestations have no evidence of either culture-

proven intraamniotic infection or intraamniotic inflammation. *Am. J. Obstet. Gynecol.* 216, 604.e1–604.e11. <https://doi.org/10.1016/j.ajog.2017.02.035>.

Olson, D.M., and Ammann, C. (2007). Role of the prostaglandins in labour and prostaglandin receptor inhibitors in the prevention of preterm labour. *Front. Biosci.* 12, 1329–1343. <https://doi.org/10.2741/2151>.

Panfoli, I., Ravera, S., Podesta, M., Cossu, C., Santucci, L., Bartolucci, M., Bruschi, M., Calzia, D., Sabatini, F., Bruschetti, M., et al. (2016). Exosomes from human mesenchymal stem cells conduct aerobic metabolism in term and preterm newborn infants. *FASEB J.* 30, 1416–1424. <https://doi.org/10.1096/fj.15-279679>.

Pines, A., Kelstrup, C.D., Vrouwe, M.G., Puigvert, J.C., Typas, D., Misovic, B., de Groot, A., von Stechow, L., van de Water, B., Danen, E.H., et al. (2011). Global phosphoproteome profiling reveals unanticipated networks responsive to cisplatin treatment of embryonic stem cells. *Mol. Cell Biol.* 31, 4964–4977. <https://doi.org/10.1128/MCB.05258-11>.

Poltorak, A., He, X., Smirnova, I., Liu, M.Y., Van Huffel, C., Du, X., Birdwell, D., Alejos, E., Silva, M., Galanos, C., et al. (1998). Defective LPS signaling in C3H/HeJ and C57BL/10ScCr mice: mutations in Tlr4 gene. *Science* 282, 2085–2088. <https://doi.org/10.1126/science.282.5396.2085>.

Purandare, N., Minchella, P., Somayajulu, M., Kramer, K.J., Zhou, J., Adekoya, N., Welch, R.A., Grossman, L.I., Aras, S., and Recanatani, M.A. (2021). Molecular mechanisms regulating lysophosphatidylcholine acyltransferase 1 (LPCAT1) in human pregnancy. *Placenta* 106, 40–48. <https://doi.org/10.1016/j.placenta.2021.02.005>.

Purandare, N., Somayajulu, M., Huttemann, M., Grossman, L.I., and Aras, S. (2018). The cellular stress proteins CHCHD10 and MNRR1 (CHCHD2): partners in mitochondrial and nuclear function and dysfunction. *J. Biol. Chem.* 293, 6517–6529. <https://doi.org/10.1074/jbc.RA117.001073>.

Rizzo, G., Mappa, I., Bitsadze, V., Khizroeva, J., Makatsariya, A., and D’Antonio, F. (2020). Administration of antenatal corticosteroid is associated with reduced fetal growth velocity: a longitudinal study. *J. Matern. Fetal Neonatal Med.* 1–6. <https://doi.org/10.1080/14767058.2020.1800634>.

Roberts, V.H., Smith, J., McLea, S.A., Heizer, A.B., Richardson, J.L., and Myatt, L. (2009). Effect of increasing maternal body mass index on oxidative and nitrate stress in the human placenta. *Placenta* 30, 169–175. <https://doi.org/10.1016/j.placenta.2008.11.019>.

Saita, S., Tatsuta, T., Lampe, P.A., Konig, T., Ohba, Y., and Langer, T. (2018). PARL partitions the lipid transfer protein STARD7 between the cytosol and mitochondria. *EMBO J.* 37. <https://doi.org/10.15252/embj.201797909>.

Seckl, J.R., Cleasby, M., and Nyirenda, M.J. (2000). Glucocorticoids, 11beta-hydroxysteroid dehydrogenase, and fetal programming. *Kidney Int.* 57, 1412–1417. <https://doi.org/10.1046/j.1523-1755.2000.00984.x>.

Sferruzzi-Perri, A.N., Higgins, J.S., Vaughan, O.R., Murray, A.J., and Fowden, A.L. (2019). Placental mitochondria adapt developmentally and in response to hypoxia to support fetal growth. *Proc. Natl. Acad. Sci. USA* 116, 1621–1626. <https://doi.org/10.1073/pnas.1816056116>.

Stavru, F., Bouillaud, F., Sartori, A., Ricquier, D., and Cossart, P. (2011). *Listeria monocytogenes* transiently alters mitochondrial dynamics during infection. *Proc. Natl. Acad. Sci. USA* 108, 3612–3617. <https://doi.org/10.1073/pnas.1100126108>.

Tiku, V., Tan, M.W., and Dikic, I. (2020). Mitochondrial functions in infection and immunity. *Trends Cell Biol.* 30, 263–275. <https://doi.org/10.1016/j.tcb.2020.01.006>.

Trnka, J., Blaikie, F.H., Smith, R.A., and Murphy, M.P. (2008). A mitochondria-targeted nitroxide is reduced to its hydroxylamine by ubiquinol in mitochondria. *Free Radic. Biol. Med.* 44, 1406–1419. <https://doi.org/10.1016/j.freeradbiomed.2007.12.036>.

Valentin-Vega, Y.A., Maclean, K.H., Tait-Mulder, J., Milasta, S., Steeves, M., Dorsey, F.C., Cleveland, J.L., Green, D.R., and Kastan, M.B. (2012). Mitochondrial dysfunction in ataxia-telangiectasia. *Blood* 119, 1490–1500. <https://doi.org/10.1182/blood-2011-08-373639>.

Vringer, E., and Tait, S.W.G. (2019). Mitochondria and inflammation: cell death heats up. *Front. Cell Dev. Biol.* 7, 100. <https://doi.org/10.3389/fcell.2019.00100>.

Wai, T., Garcia-Prieto, J., Baker, M.J., Merkwirth, C., Benit, P., Rustin, P., Ruperez, F.J., Barbas, C., Ibanez, B., and Langer, T. (2015). Imbalanced OPA1 processing and mitochondrial

fragmentation cause heart failure in mice. *Science* 350, aad0116. <https://doi.org/10.1126/science.aad0116>.

Wang, Y., Bucher, M., and Myatt, L. (2019). Use of glucose, glutamine and fatty acids for trophoblast respiration in lean, obese and gestational diabetic women. *J. Clin. Endocrinol. Metab.* <https://doi.org/10.1210/jc.2019-00166>.

Wapner, R.J., Sorokin, Y., Mele, L., Johnson, F., Dudley, D.J., Spong, C.Y., Peaceman, A.M., Leveno, K.J., Malone, F., Caritis, S.N., et al. (2007). Long-term outcomes after repeat doses of antenatal corticosteroids. *N. Engl. J. Med.* 357, 1190–1198. <https://doi.org/10.1056/NEJMoa071453>.

Weintz, G., Olsen, J.V., Fruhauf, K., Niedzielska, M., Amit, I., Jantsch, J., Mages, J., Frech, C., Dolken, L., Mann, M., and Lang, R. (2010). The phosphoproteome of toll-like receptor-activated macrophages. *Mol. Syst. Biol.* 6, 371. <https://doi.org/10.1038/msb.2010.29>.

West, A.P., Brodsky, I.E., Rahner, C., Woo, D.K., Erdjument-Bromage, H., Tempst, P., Walsh, M.C., Choi, Y., Shadel, G.S., and Ghosh, S. (2011). TLR signalling augments macrophage bactericidal activity through mitochondrial ROS. *Nature* 472, 476–480. <https://doi.org/10.1038/nature09973>.

Wu, Q., Allouch, A., Paoletti, A., Leteur, C., Mirjolet, C., Martins, I., Voisin, L., Law, F., Dakhli, H., Mintet, E., et al. (2017). NOX2-dependent ATM kinase activation dictates pro-inflammatory macrophage phenotype and improves effectiveness to radiation therapy. *Cell Death Differ.* 24, 1632–1644. <https://doi.org/10.1038/cdd.2017.91>.

Yang, J., Staples, O., Thomas, L.W., Briston, T., Robson, M., Poon, E., Simoes, M.L., El-Emir, E., Buffa, F.M., Ahmed, A., et al. (2012). Human CHCHD4 mitochondrial proteins regulate cellular oxygen consumption rate and metabolism and provide a critical role in hypoxia signaling and tumor progression. *J. Clin. Invest.* 122, 600–611. <https://doi.org/10.1172/JCI58780>.

Yung, H.W., Colleoni, F., Dommett, E., Cindrova-Davies, T., Kingdom, J., Murray, A.J., and Burton, G.J. (2019). Noncanonical mitochondrial unfolded protein response impairs placental oxidative phosphorylation in early-onset preeclampsia. *Proc. Natl. Acad. Sci. USA* 116, 18109–18118. <https://doi.org/10.1073/pnas.1907548116>.

Zhang, K., Shen, X., Wu, J., Sakaki, K., Saunders, T., Rutkowski, D.T., Back, S.H., and Kaufman, R.J. (2006). Endoplasmic reticulum stress activates cleavage of CREBH to induce a systemic inflammatory response. *Cell* 124, 587–599. <https://doi.org/10.1016/j.cell.2005.11.040>.

Zheng, C., Zhou, Y., Huang, Y., Chen, B., Wu, M., Xie, Y., Chen, X., Sun, M., Liu, Y., Chen, C., and Pan, J. (2019). Effect of ATM on inflammatory response and autophagy in renal tubular epithelial cells in LPS-induced septic AKI. *Exp. Ther. Med.* 18, 4707–4717. <https://doi.org/10.3892/etm.2019.8115>.

Zhong, F., Liang, S., and Zhong, Z. (2019). Emerging role of mitochondrial DNA as a major driver of inflammation and disease progression. *Trends Immunol.* 40, 1120–1133. <https://doi.org/10.1016/j.it.2019.10.008>.

STAR★METHODS

KEY RESOURCES TABLE

REAGENT or RESOURCE	SOURCE	IDENTIFIER
<i>Antibodies</i>		
α -Actin	Cell Signaling Technology	Cat # 12748; RRID:AB_2798015
α -ATM	Cell Signaling Technology	Cat # 2873; RRID:AB_2062659
α -DRBP76	Proteintech	Cat # 19887-1-AP; RRID:AB_10666431
α -FLAG	Sigma	Cat # A8592; RRID:AB_439702
α -GAPDH	Cell Signaling Technology	Cat # 8884; RRID:AB_11129865
α -I κ B α	Cell Signaling Technology	Cat # 4814; RRID:AB_390781
α -Lamin	Santa Cruz Biotechnology	Cat # sc-30264 RRID:AB_2136305
α -MNRR1	Proteintech	Cat # 19424-1-AP; RRID:AB_10638907
α -MNRR1 (used for immunostaining human cells)	Proteintech	Cat # CL594-66302; RRID:AB_2883552
α -Mouse secondary HRP conjugate	Cell Signaling Technology	Cat # 7076; RRID:AB_330924
α -MTCO2	Proteintech	Cat # 55070-1-AP; RRID:AB_10859832
α -NOX2	Proteintech	Cat # 19013-1-AP; RRID:AB_2833044
α -Phospho-CHK2 (T68)	Cell Signaling Technology	Cat # 2197; RRID:AB_2080501
α -phospho-JNK (T183/Y185)	Cell Signaling Technology	Cat # 4668; RRID:AB_823588
α -phospho-TBK1	Cell Signaling Technology	Cat # 5483; RRID:AB_10693472
α -phospho-threonine	Cell Signaling Technology	Cat # 9368; RRID:AB_10693777
α -phospho-threonine agarose conjugate beads	Santa Cruz Biotechnology	Cat # sc-5267; RRID:AB_628121
α -Rabbit secondary HRP conjugate	Cell Signaling Technology	Cat # 7074; RRID:AB_2099233
α -Rabbit Alexa 594 conjugate	Jackson Labs	Cat # 711-585-152; RRID:AB_2340621
α -RELA/p65	Proteintech	Cat # 10745-1-AP; RRID:AB_2178878
α -STARD7	Proteintech	Cat # 15689-1-AP; RRID:AB_2197820
α -TLR4 (used for human cells)	Santa Cruz Biotechnology	Cat # sc-293072 RRID:AB_10611320

(Continued on next page)

Continued

REAGENT or RESOURCE	SOURCE	IDENTIFIER
α -TLR4 (used for mouse tissue)	Proteintech	Cat # 19811-1-AP; RRID:AB_10638446
α -TOM20 (used for immunostaining human cells)	Proteintech	Cat # CL488-11802
α -total CHK2	Cell Signaling Technology	Cat # 6334; RRID:AB_11178526
α -total JNK	Cell Signaling Technology	Cat # 9252; RRID:AB_2250373
α -total TBK1	Cell Signaling Technology	Cat # 3504; RRID:AB_2255663
α -Tubulin	Cell Signaling Technology	Cat # 9099; RRID:AB_10695471
α -YME1L1	Proteintech	Cat # 11510-1-AP; RRID:AB_2217459
Protein L-agarose beads (used for p-threonine IP)	Santa Cruz Biotechnology	Cat # sc-2336
Protein A/G agarose beads (used for YME1L1-IP)	Santa Cruz Biotechnology	Cat # sc-2003

Biological samples

Human systemic inflammation placental samples (base plate and villi)	Perinatology Research Branch, an intramural program of the Eunice Kennedy Shriver NICHD, NIH, DHHS, Wayne State University (Detroit, MI, USA), and the Detroit Medical Center (Detroit, MI, USA)	NA
Mouse placental tissues and tissue sections	Perinatology Research Branch, an intramural program of the Eunice Kennedy Shriver NICHD, NIH, DHHS, Wayne State University (Detroit, MI, USA), and the Detroit Medical Center (Detroit, MI, USA)	NA
WT and Myd88 ^{-/-} mouse liver tissues and WT and TLR4 ^{-/-} liver tissue lysates	Dr. Kezhong Zhang, Wayne State University	NA

Chemicals, peptides, and recombinant proteins

ATM inhibitor (KU-55933)	Cell Signaling Technology	Cat # 83346S
Clotrimazole	Selleck Chem	Cat #S1606
Lipopolysaccharide <i>Escherichia coli</i> O 111:B4 (used for human cells)	Invivogen	Cat # tlrl-3pelps
Lipopolysaccharide <i>Escherichia coli</i> O 111:B4 (used for mouse injections)	Sigma	Cat # L6259
N-acetylcysteine	Sigma	Cat # A7250
Nitazoxanide	Selleck Chem	Cat # S1627
NOX2 inhibitor (GSK2795039)	Selleck Chem	Cat # S8974

Critical commercial assays

Cell Titer Glo	Promega	Cat # G7572
CM-H ₂ DCFDA	Thermo Fisher	Cat # C6827
Dual luciferase reporter assay system	Promega	Cat # E1910
Endo-free plasmid purification kit	Qiagen	Cat # 12362
Mitochondrial fractionation kit	Thermo Fisher	Cat # 89874
MitoSOX Red	Thermo Fisher	Cat # M36008

(Continued on next page)

Continued

REAGENT or RESOURCE	SOURCE	IDENTIFIER
Protoscript II cDNA synthesis kit	New England Biolabs	Cat # E6560
QuikChange Lightning Site-Directed Mutagenesis Kit	Agilent	Cat # 210518
RNAeasy RNA isolation kit	Qiagen	Cat # 74134
Transfast transfection reagent	Promega	Cat # E2431

Experimental models: Cell lines

BeWo	Perinatology Research Branch, an intramural program of the Eunice Kennedy Shriver NICHD, NIH, DHHS, Wayne State University (Detroit, MI, USA), and the Detroit Medical Center (Detroit, MI, USA)	RRID:CVCL_0044
HEK293-WT and YME1L1 ^{-/-}	Dr. Thomas Langer	(MacVicar et al., 2019)
HTR8 SV/neo	Perinatology Research Branch, an intramural program of the Eunice Kennedy Shriver NICHD, NIH, DHHS, Wayne State University (Detroit, MI, USA), and the Detroit Medical Center (Detroit, MI, USA)	RRID:CVCL_7162
JAR	ATCC	Cat # HTB-144; RRID:CVCL_0360

Experimental models: Organisms/strains

C57BL/6	The Jackson Laboratory	Stock# 000664
---------	------------------------	---------------

Recombinant DNA

MNRR1-C-S-pCI-Neo (all 4 cysteines mutated to Serine)	Described previously	(Aras et al., 2015)
MNRR1-pGL3 basic (Firefly luciferase reporter)	Described previously	(Aras et al., 2020)
MNRR1-WT-pCI-Neo	Described previously	(Aras et al., 2013)
MNRR1-Y99E-pCI-Neo	Described previously	(Aras et al., 2017)
MNRR1-Y99F-pCI-Neo	Described previously	(Aras et al., 2017)
PRL-SV40 (<i>Renilla</i> luciferase)	Described previously	(Aras et al., 2013, 2017; Purandare et al., 2018)
hTLR4-pcDNA3.1	Addgene	RRID:Addgene_13086
YME1L1-E543Q-pCDNA5 (protease-dead)	Dr. Thomas Langer	(MacVicar et al., 2019)
YME1L1-T695A-pCDNA5	Generated in this study	NA
YME1L1-T656A-pCDNA5	Generated in this study	NA
YME1L1-WT-pCDNA5	Dr. Thomas Langer	(MacVicar et al., 2019)

Software and algorithms

MStat	N. Drinkwater (McArdle Lab, University of Wisconsin-Madison)
Volocity	Perkin-Elmer

RESOURCE AVAILABILITY

Lead contact

Further information and requests for resources and reagents should be directed to and will be fulfilled by the lead contact, Lawrence Grossman (lgrossman@wayne.edu).

Materials availability

All unique reagents generated from this study are available from the [lead contact](#) with a completed Materials Transfer Agreement.

Data and code availability

This study did not generate original code. Any additional information required to reanalyze the data reported in this paper is available from the [lead contact](#) upon request.

METHODS DETAILS

Cell culture and reagents

Cell lines

All cell media were supplemented with 10% fetal bovine serum (FBS) (Sigma Aldrich, St. Louis, MO) plus Penicillin-Streptomycin (HyClone). HTR8/SVneo (HTR), and JAR cells were cultured in Roswell Park Memorial Institute Medium (RPMI) (HyClone). The BeWO cells were grown in F12K media (Gibco). HEK293 cells were grown in Dulbecco's modified Eagle's medium (without pyruvate). YME1L1 knockout-HEK293 cells were grown in Dulbecco's modified Eagle's medium (with 1 mM pyruvate) supplemented with non-essential amino acids (Gibco).

Chemicals

Nitazoxanide and Clotrimazole were obtained from Selleckchem and solubilized in DMSO (used as vehicle control in all experiments with these compounds). Ultrapure LPS for cell culture experiments (Lipopolysaccharide from *Escherichia coli* 0111:B4) was purchased from Invivogen. NOX2 inhibitor GSK2795039 was obtained from MedChem Express. ATM inhibitor KU-55933 was from Cell Signaling Technology.

Plasmids

The WT and protease dead (PD) YME1L1 plasmids were a kind gift from Dr. Thomas Langer, University of Cologne, DE. The *MNRR1* promoter luciferase reporter plasmid has been described previously (Aras et al., 2015). hTLR4 was a gift from Dr. Ruslan Medzhitov, Yale University (Addgene plasmid # 13086; <http://n2t.net/addgene:13,086>; RRID:Addgene_13086). The T695A and T656A mutations were generated in WT-YME1L1 plasmid via QuikChange Lightning Site-Directed Mutagenesis Kit (Agilent) and confirmed by sequencing. All the expression plasmids were purified using the Endo-Free plasmid purification kit from Qiagen.

Transient transfection of HTR cells

HTR cells were transfected with the indicated plasmids using TransFast transfection reagent (Promega) according to the manufacturer's protocol. A TransFast:DNA ratio of 3:1 in serum and antibiotic free medium was used. Following incubation at room temperature for ~15 min, the cells were overlaid with the mixture. The plates were incubated for 1 h at 37°C followed by replacement with complete medium and further incubation for the indicated time.

Real-time PCR

Total cellular RNA was extracted from mouse placental tissue or HTR cells with an RNeasy Plus Mini Kit (Qiagen) according to the manufacturer's instructions. Complementary DNA (cDNA) was generated by reverse transcriptase polymerase chain reaction (PCR) using the ProtoScript® II First Strand cDNA Synthesis Kit (New England Biolabs). Transcript levels were measured by real time PCR using SYBR green on an ABI 7500 system. Real-time analysis was performed by the $\Delta\Delta^{Ct}$ method as previously (Purandare et al., 2018). The primer sequences used have been included as [Table S1](#).

Luciferase reporter assay

Luciferase assays were performed with the dual-luciferase reporter assay kit (Promega). Briefly, cells were lysed in 1x passive lysis buffer (Promega) and 25 μ L of lysate was used for assay with a tube luminometer using an integration time of 10 s. Transfection efficiency was normalized with the co-transfected pRL-SV40 *Renilla* luciferase expression plasmid (Aras et al., 2013, 2017; Purandare et al., 2018).

Intact cellular oxygen consumption

Cellular oxygen consumption was measured with a Seahorse XF^e24 Bioanalyzer (Agilent). Cells were plated at a concentration of 3×10^4 per well a day prior to treatment and basal oxygen consumption was measured 24 h after treatments as described (Aras et al., 2017; Purandare et al., 2018).

ATP measurements

2.5 × 10⁴ HTR cells per well were plated in a 96-well plate a day prior to treatment and ATP levels were measured using Cell Titer Glo (Promega) according to manufacturer's instructions. Cells were lysed in 100 μL of reagent, mixed for 2 min to induce lysis, and incubated for 10 min to stabilize the signal. Luminescence was recorded using a BioTek Synergy H1 Microplate Reader (Agilent).

ROS measurements

Total cellular ROS measurements were performed with CM-H₂DCFDA (Life Technologies). Cells were distributed into 96-well plates at 2.5 × 10⁴ cells per well and incubated for 24 h or as described in specific experiments. Cells were then treated with 10 μM CM-H₂DCFDA in serum- and antibiotic-free medium for 1 h. Cells were washed twice in phosphate buffered saline and analyzed for fluorescence on a BioTek Synergy H1 Microplate Reader (Agilent). For mitochondrial ROS measurements, the cells were treated as above but with 5 μM MitoSox Red (Life Technologies) for 30 min.

Confocal microscopy

Confocal microscopy was performed as described (Aras et al., 2017; Purandare et al., 2018). For mouse placental tissue sections, 8–10 μm thick transverse sections were fixed with 4% paraformaldehyde and were stained with anti-MNRR1 antibody (1:50 Proteintech) overnight at 4°C. The secondary antibody used was donkey anti-rabbit IgG Alexa 594 (1:200, Jackson Labs, Bar Harbor, ME) for 1 h. Human placental cells were grown on glass coverslips and fixed with 4% paraformaldehyde. Staining was performed with anti-MNRR1 (1:50 Proteintech) conjugated to CoraLite-594 and anti-TOM20 conjugated to CoraLite-488 (1:200, Proteintech) overnight at 4°C.

Cells were imaged with a Leica TCS SP5 microscope and images were combined in Photoshop. Intensity (number of pixels per unit area) for the tissue sections were quantitated using Volocity image analysis software (Perkin Elmer).

Mitochondria isolation

Mitochondria were isolated from cells with a Mitochondrial Isolation Kit (Thermo Scientific, Rockford, IL) per manufacturer's protocol (Aras et al., 2017; Purandare et al., 2018). Briefly, the cells were treated with a hypotonic lysis buffer and the nuclear fraction was obtained by low-speed centrifugation. The pellet was washed twice with PBS to obtain enriched nuclei. The mitochondrial fraction was obtained after high-speed centrifugation of the nuclear supernatant and washed with a sucrose containing isotonic buffer to prevent lysis. Cross-contamination between the fractions was determined with compartment-specific antibodies – DRBP76 for nuclei and MTCO2 for mitochondria.

Immunoblotting and co-immunoprecipitation

Immunoblotting was performed as described previously (Aras et al., 2013, 2015). Cell lysates for immunoblotting were prepared using 2% CHAPS in Tris-buffered saline (TBS; 25 mM Tris, 0.15 M NaCl; pH 7.2) and tissue lysate were prepared using 50 mM Tris-HCl (pH 8.0) with 150 mM NaCl, 1% NP-40, 0.5% sodium deoxycholate and 0.1% SDS. All lysis buffers included a protease and phosphatase inhibitor cocktail (Sigma, PPC1010). Total protein extracts were obtained by centrifugation at 21000 xg for 30 min at 4°C. The clear supernatants were transferred to new tubes and quantified using the Bradford reagent with BSA as standard (BioRad). Equal amounts of cell lysates were separated by sodium dodecyl sulphate–polyacrylamide gel electrophoresis (SDS–PAGE), transferred to PVDF membranes (BioRad), and blocked with 5% non-fat dry milk. Incubation with primary antibodies (used at a concentration of 1:500) was performed overnight at 4°C. Incubation with secondary antibodies (1:5000) was performed for 2 h at room temperature. For detection post-immunoblotting, the SuperSignal™ West Pico PLUS substrate (ThermoFisher) was used to generate a chemiluminescence signal, which was detected with X-ray film (RadTech).

Immunoprecipitation experiments were performed according to the supplier's protocol by incubating the antibody-adsorbed beads overnight at 4°C. For immunoprecipitation experiments, cells were lysed in 50 mM Tris buffer, pH 7.4, containing 150 mM NaCl, 0.1% Triton X-100, 1 mM sodium orthovanadate, 10 mM NaF, 10 mM β-glycerophosphate, 5 mM sodium pyrophosphate, and protease and phosphatase inhibitor cocktail (Sigma, PPC1010). Phosphothreonine antibody (Cell Signaling) conjugated to

L-agarose beads (sc-2336, SCBT) or YME1L1 antibody (Proteintech) conjugated to protein A/G-agarose beads (sc-2003, SCBT) were used.

Animal experiments and injections

Mouse placental samples were obtained using the intraperitoneal injection LPS (*E. coli* O 111:B4; Sigma) model that results in preterm labor/birth (Gomez-Lopez et al., 2018). Briefly, pregnant B6 mice were intraperitoneally injected on 16.5 dpc with 15 μ g of LPS in 200 μ L of PBS using a 26-gauge needle. Controls were injected with 200 μ L of PBS. Mice were monitored via video recording using an infrared camera to determine gestational age and the rate of preterm labor. Placentas were collected before preterm birth (12–13 h after LPS injection).

For preparation of mouse liver samples for Myd88^{-/-} and TLR4^{-/-} involvement, mice of approximately 3-months were injected intraperitoneally with LPS (*E. coli* O 111:B4, Sigma, 2 μ g/gm body weight) or PBS for 18 h (Dandekar et al., 2016). Liver tissues collected from the mice after LPS treatment were homogenized in NP-40 lysis buffer in the presence of proteasome inhibitors. Lipid contents were briefly extracted from the liver tissue lysates by the SDS buffer, and the protein supernatants were denatured for Western blot analyses (Zhang et al., 2006).

All animal procedures were approved by the Institutional Animal Care and Use Committee (IACUC) at Wayne State University under Protocol No. A-07-03-15.

QUANTIFICATION AND STATISTICAL ANALYSIS

Statistical analyses were performed with MSTAT version 6.1.1 (N. Drinkwater, University of Wisconsin, Madison, WI). The two-sided Wilcoxon rank-sum test was applied to determine statistical significance for p values. Data were considered statistically significant with p < 0.05. Error bars represent standard error of mean.